ACS APPLIED ENERGY MATERIALS

www.acsaem.org Article

Discovery of a Hybrid System for Photocatalytic CO_2 Reduction via Attachment of a Molecular Cobalt-Quaterpyridine Complex to a Crystalline Carbon Nitride

Scott McGuigan, Stephen J. Tereniak, Carrie L. Donley, Avery Smith, Sungho Jeon, Fengyi Zhao, Renato N. Sampaio, Magnus Pauly, Landon Keller, Leonard Collins, Gregory N. Parsons, Tianquan Lian, Eric A. Stach, and Paul A. Maggard*

Cite This: *ACS Appl. Energy Mater.* 2023, 6, 10542−10553 Read Online

ACCESS | Metrics & More | Article Recommendations | Supporting Information

ABSTRACT: While recent reports have demonstrated the attachment of molecular catalysts to amorphous, graphitic carbon nitrides (g-CN) for light-driven CO_2 reduction, approaches to the utilization of crystalline carbon nitrides have remained undiscovered. Herein, a functional hybrid photocatalyst system has been found using a crystalline carbon nitride semiconductor, poly(triazine imide) lithium chloride (PTI-LiCl), with a surface-attached $CoCl_2$(qpy-Ph-COOH) catalyst for CO_2 reduction. The molecular catalyst attaches to PTI-LiCl at concentrations from 0.10 to 4.30 wt % and exhibits ∼96% selectivity for CO production in a CO_2-saturated, aqueous 0.5 M $KHCO_3$ solution. Optimal loadings were found to be within 0.42−1.04 wt % with rates between 1,400 and 1,550 μmol CO/g·h at an irradiance of 172 mW/cm^2 (λ = 390 nm) and apparent quantum yields of ∼2%. This optimized loading is postulated to represent a balance between maximal turnover frequency (TOF; 300+ h^{-1}) and excess catalyst that can limit excited-electron lifetimes, as probed via transient absorption spectroscopy. An increase in the incident irradiance yields a concomitant increase in the TOFs and CO rates only for the higher catalyst loadings, reaching up to 2,149 μmol CO/g·h with a more efficient use of the catalyst surface capacity. The lower catalyst loadings, by comparison, already function at maximal TOFs. Higher surface loadings are also found to help mitigate deactivation of the molecular catalysts during extended catalytic testing (>24 h) owing to the greater net surface capacity for CO_2 reduction, thus representing an effective strategy to extend lifetime. The hybrid particles can be deposited onto an FTO substrate to yield ∼60% Faradaic efficiency for photoelectrochemical CO production at −1.2 V vs Ag/AgCl bias. In summary, these results demonstrate the synergistic combination of a crystalline carbon nitride with a molecular catalyst that achieves among the highest known rates in carbon-nitride systems for the light-driven CO_2 reduction to CO in aqueous solution with >95% selectivity.

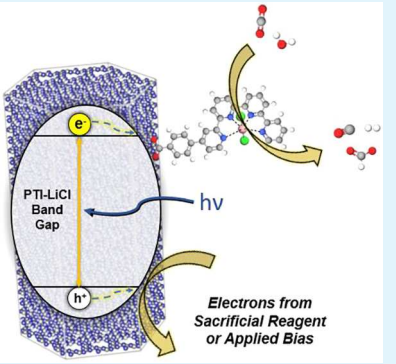

KEYWORDS: *hybrid materials, photocatalysis, carbon nitride, CO_2 reduction*

INTRODUCTION

Anthropogenic activity is leading to an escalation in the detrimental climate change of our planet stemming from nonrenewable fuel consumption and various industrial processing methods that release CO_2 and other harmful greenhouse gases.[1,2] A major current research thrust involves the development of semiconductors exhibiting band gaps that enable efficient solar energy conversion to chemical fuels, such as especially via molecular catalysts attached to their surfaces.[3,4] Within this area, polymeric carbon nitride (i.e., PCN) semiconductors that consist of covalently linked carbon nitride layers with varying amounts of hydrogen have come under intense investigation. Their advantages include modest bandgap energies that extend into the visible-light wavelengths (∼2.5 to 3.1 eV) as well as suitable band edge energies to drive both CO_2 or H_2O reduction. As compared to purely inorganic semiconductors, they also offer a greater kinetic stability and underlying structural tunability with the use of molecular precursors and low-temperature reaction conditions.[5,6] The native surfaces of PCN semiconductors have demonstrated a capacity toward functionalization with diverse molecular catalysts with the aim to increase product selectivity and lower reaction activation barriers, as is nearly always associated with thermodynamically uphill multielectron processes such as overall water splitting.[7−9]

Most notably, graphitic-CN (g-CN; band gap ∼2.7 eV) has been intensely investigated in recent years as a semiconductor

Received: July 5, 2023
Accepted: September 12, 2023
Published: October 12, 2023

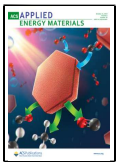

Scheme 1. Schematic for the Preparation of the Hybrid Molecular Catalyst/Carbon Nitride Semiconductor System, i.e., $CoCl_2$(qpy-Ph-COOH)/PTI-LiCl, Involving the Preparation of PTI-LiCl and Attachment of the Catalyst from a Solution[a]

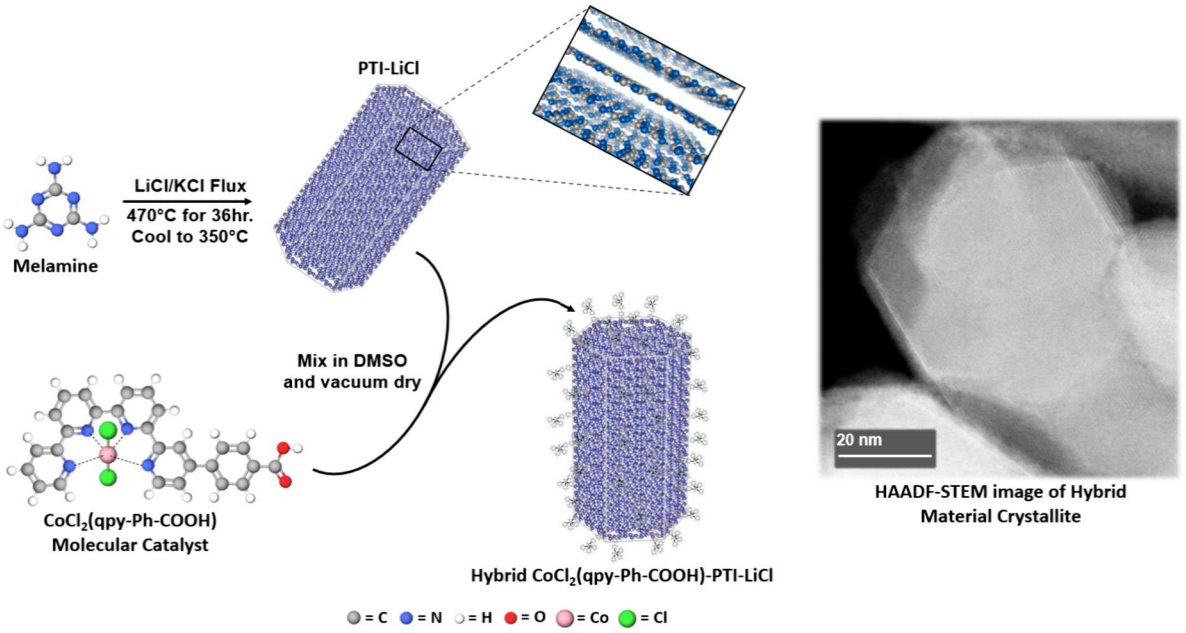

[a]A representative HAADF-STEM image is shown (right). Coordinated Li and Cl ions in the PTI framework are omitted for clarity.

scaffolding for enabling solar energy conversion, with many studies aimed at the attachment of molecular catalysts to its surfaces.[10] Because of its inherent $-NH_x$ surface functional groups and covalently bonded structure, many common attachment strategies for molecular catalysts have been found and include the use of complementary carboxylates, phosphonates, π-based systems, and other functional substituents of derivatized catalyst ligands. Recent examples have primarily focused on the attachment of metal-coordinated (e.g., M = Fe, Co, Mn, and Ru) phthalocyanine-, bipyridyl-, and quaterpyridyl-based complexes to the surfaces of g-CN.[11−16] These hybrid materials have shown increasingly promising rates for the light-driven catalytic reduction of CO_2, predominantly to CO and/or formate. However, photocatalytic CO_2 reduction in nearly all of these prior studies has occurred in saturated organic solvents, such as acetonitrile or *N*,*N*-dimethylacetamide, rather than aqueous solutions. Further, the reported molecular catalysts' turnover number (TON) and turnover frequency (TOF) when attached to g-CN are both orders of magnitude smaller as compared to when the same catalyst is measured under applied bias at a conducting electrode surface. For example, a cobalt-quaterpyridine complex exhibits selective electrocatalytic reduction of CO_2 to CO (~97 to 100% selectivity), with a near-record TOF of 1.9×10^6 h^{-1} at 0.14 V overpotential in acetonitrile. However, the same catalyst shows a significantly lower 2.1×10^4 h^{-1} TOF (TON = 42,960) at 0.34 V overpotential in water.[17,18] Use of the same Co−quaterpyridine catalyst attached to g-CN, via a −COOH functional group, yields a meager TOF of ~5 h^{-1} (TON ≈ 500) in acetonitrile solution with 98% selectivity.[14] This compares to the photon flux of sunlight (AM 1.5G) of ~15 photons/nm^2·s that requires a catalyst TOF of $\sim 1.1 \times 10^6$ h^{-1}, similar to those of known molecular catalysts, assuming an average surface coverage of 0.5 catalyst molecules per nm^2. Thus, while the g-CN scaffolding can typically maintain the molecular catalyst selectivity, new approaches are urgently needed to enable the semiconductor to facilitate higher CO_2 reduction rates and TOFs.

Owing to the relatively amorphous character of g-CN and its high defect concentration, it is well-known to be plagued by charge trapping and relatively fast rates of electron−hole recombination.[19,20] This major issue inhibits its efficacious use with surface-based molecular catalysts, thus representing a critical bottleneck and limiting the overall photocatalytic efficiency. Among the possible strategies to address defect mitigation is the utilization of a more highly crystalline PCN, i.e., poly(triazine imide) (PTI-LiCl), that has recently been discovered using molten salt techniques.[21−23] Molten salt mixtures such as LiCl/KCl serve as the medium for the condensation of small molecule precursors, e.g., urea and melamine, into crystalline PCNs at temperatures of ~470 to 550 °C. Tuning of the synthetic conditions has enabled the minimization of deleterious defects that mediate charge recombination and its more efficient use as a semiconductor scaffolding.[24] Recently, record-level apparent quantum yields of 12 to 20% for PTI-LiCl have been achieved for overall water splitting and a durability of >24 h with the attachment of surface-based inorganic catalysts (e.g., CoO_x and Pt/Cr_2O_3).[9,24] However, the development of crystalline PTI-LiCl for light-driven CO_2 reduction with the use of surface-attached molecular catalysts has so far not been demonstrated.

Reported herein is the synthesis and efficacious attachment of the cobalt-quaterpyridine catalyst, $CoCl_2$(qpy-Ph-COOH), to the surfaces of crystalline PCN, PTI-LiCl, through a carboxylic acid functional group. A schematic of this hybrid system is shown in Scheme 1 and in Figure S20a, which has been characterized by a range of experimental techniques, including X-ray photoelectron spectroscopy (XPS), scanning/transmission electron microscopy (S/TEM), and transient absorption spectroscopy (TAS). By varying the weight loading of the molecular catalyst and the incident irradiance, this

https://doi.org/10.1021/acsaem.3c01670
ACS Appl. Energy Mater. 2023, 6, 10542−10553

system is found to exhibit the currently highest known rates and selectivity for light-driven reduction of CO_2 to CO using PCNs in aqueous solution. This hybrid material is additionally capable of adhering to substrates, e.g., FTO slides, through an electrophoretic deposition process that removes the need for sacrificial reagents. Thus, this study unveils the effective combination of a crystalline carbon nitride semiconductor with a surface-based molecular catalyst for the selective reduction of CO_2 to CO under irradiation in aqueous solutions.

EXPERIMENTAL SECTION

Synthetic Preparation of the Co-Quaterpyridine/PTI-LiCl Hybrid System. First, crystalline PTI-LiCl was synthesized according to a previously reported procedure.[23] Briefly, melamine powder (1.000g) was ground in a mortar and pestle with a LiCl (0.933g) and KCl (1.327g) eutectic salt flux mixture (1:5 mol ratio of melamine to LiCl/KCl flux) until homogeneous. This mixture was then dried in an oven at 140 °C overnight. This mixture was then immediately transferred to a fused-silica reaction vessel with a high volume (~80 mL total volume) to help minimize pressure buildup from the ammonia liberation during the reaction. The sealed reaction vessel was then placed in a muffle furnace and heated to 470 °C at a rate of 7−8 °C/min, soaked at that temperature for 36 h, and then cooled to 350 °C at a rate of 2 °C h^{-1}. The reaction mixture was then allowed to radiatively cool to room temperature. The product was isolated from the vessel and washed several times in DI water to remove residual salt flux followed by a final wash in acetone and drying at room temperature. The product was characterized using powder X-ray diffraction (PXRD) on a Rigaku R-Axis Spider with CuKα radiation (λ = 1.54056 Å) from a sealed tube X-ray source (40 kV, 36 mA) and a curved image-plate detector. UV−vis diffuse reflectance (DR) spectra were collected on a Shimadzu UV-3600 UV−vis-NIR spectrophotometer with an integration sphere range of 250−1000 nm and pressed $BaSO_4$ disks as the reflectance backgrounds. Fourier-transform infrared spectroscopy (FT-IR) was used to collect spectra on a Cary 630 Agilent Spectrometer in the range of 4,000 to 650 cm^{-1}. The characterization data are shown in Figure S1.

Next, a four-step preparation of the carboxylate-functionalized quaterpyridine ligand, i.e., 4-([2,2′:6′,2″:6″,2‴-quaterpyridin]-4-yl)-benzoic acid (qpy-Ph-COOH), was adapted from literature procedures as described in detail in the Supporting Information.[14] Construction of the unsymmetrical quaterpyridine core was accomplished by two one-pot bromopolypyridine stannylation/Stille coupling sequences with 2,6- or 2,4-dibromopyridine, respectively, the first starting from commercially available 6-bromo-2,2′-bipyridine to furnish 6-bromo-2,2′:6′,2″-terpyridine and the second starting from the aforementioned terpyridine to afford 4-bromo-2,2′:6′,2″:6″,2‴-quaterpyridine. The 4-benzoatequaterpyridine methyl ester was delivered via Suzuki coupling of 4-methoxycarbonylphenylboronic acid with the bromoquaterpyridine, and subsequent base hydrolysis yielded the desired ligand qpy-Ph-COOH. The subsequent coordination of $CoCl_2$ and the purification of the molecular $CoCl_2$(qpy-Ph-COOH) complex were performed according to the literature.[14]

Finally, the $CoCl_2$(qpy-Ph-COOH) complex was loaded onto the PTI-LiCl powder in stoichiometric ratios from a DMSO solution (242 μM molecular catalyst). For the catalyst loading, 20−70 mg of PTI-LiCl was dispersed into 4−10 mL of the DMSO solution with the dissolved $CoCl_2$(qpy-Ph-COOH) complex to yield a nominal weight fraction for the latter of 0.10 to 4.03 wt % when isolated with PTI-LiCl. Additional DMSO was added as needed to provide the minimum of 4 mL of mixing solution. This dispersion was subject to vacuum drying on a Schlenk line until all of the DMSO solvent had evaporated and condensed within a separate liquid-N_2 cold trap. The hybrid product was thereby isolated and characterized using an array of techniques, including FT-IR, XPS, and electron microscopy (SEM and S/TEM). The XPS data was collected on a Kratos Supra+ system with a monochromatic Kα X-ray source operated at 150 W. A charge neutralizer was used to prevent charging when necessary, and all spectra were corrected to the C 1s peak at 284.6 eV. Survey and high-resolution scans were acquired at pass energies of 80 and 20 eV, respectively, and the analyzed spot size was 300 × 700 μm. The SEM images were taken using an FEI Verios 460L field-emission scanning electron microscope as an ultrahigh resolution Schottky emitter and an Oxford energy-dispersive X-ray spectrometer. The S/TEM and accompanying EDS data were taken using a JEOL NEOARM S/TEM, equipped with a spherical aberration corrector for the probe forming optics and equipped with two large area energy-dispersive X-ray spectrometers. The TEM images and the selected area diffraction patterns (SAED) were taken using a JEOL F200. We operated both S/TEM instruments at low dose mode. A NEOARM was operated at 200 kV, a 9C probe size, a 40 μm condenser lens aperture, and a 4 cm camera length yielding ~10 pA probe current. The JEOL F200 was operated at 200 kV, and the dose rate was around 10 pA/cm^2.

Photocatalytic CO_2 Reduction Experiments. Photocatalysis measurements were taken using the hybrid $CoCl_2$(qpy-Ph-COOH)/PTI-LiCl powders suspended in an aqueous bicarbonate solution. For each test, approximately 12 mg of sample was suspended in a quartz reaction vessel (total volume ~32 mL) with 10 mL of a 0.5 M $KHCO_3$ solution and adding ~0.2 M Na_2SO_3 (0.2521g) as the sacrificial electron donor to the solution unless otherwise specified. The solution was then purged for 30 min with CO_2 followed by a 5 min venting of the headspace to allow for solution equilibration and removal of residual air from the vessel. A water bubble was deposited using a glass pipet within the outlet of the reaction vessel to maintain an air-free reaction environment. This powder suspension was stirred with a magnetic bar and irradiated using a 390 nm P-160L Kessil LED lamp for a total of 4 h of reaction time unless otherwise indicated. Gas samples were taken of the reaction headspace after the first hour of headspace equilibration and at other designated intervals and injected into an SRI 8610C gas chromatograph with Ar carrier gas for product identification. Standardized gas measurements of H_2, CO, and CO_2 were used to calibrate the retention times and product quantification. Aliquots of the reaction solution were also checked by ^{1}H NMR spectroscopy. For this, liquid samples (250 μL) were taken and mixed with both D_2O (100 μL) and a standard 0.00028 M 3-(trimethylsilyl)-1-propanesulfonic acid sodium salt (DSS) solution (250 μL). These mixtures were analyzed on a Bruker Avance NEO 600 MHz NMR.

The hybrid semiconductor-molecular catalyst material was also photoelectrochemically tested after being electrophoretically deposited onto FTO glass. In the first step, ~10 mg of the hybrid powder (isolated from a DMSO solution mix with 3.6 mg of dissolved $CoCl_2$(qpy-Ph-COOH) and 80.3 mg of PTI-LiCl) was dispersed into ~11 mL of aqueous 0.5 M $KHCO_3$ solution in the cathodic compartment (~20 mL) of an H-cell for its electrophoretic deposition onto an FTO glass slide serving as the working electrode and Ag/AgCl as the reference electrode. A Pt counter electrode was used within the anodic compartment. A bias of −1.2 V vs Ag/AgCl was applied using a Pine Research Instruments WaveNow wireless or Wavenumber 200 potentiostat for 2 h to electrophoretically deposit the hybrid particles. Films were deposited with and without light irradiation from a 390 nm LED lamp, with no evidence that irradiation during deposition has an impact on the obtained film's appearance or activity. After the deposition of the hybrid particles, the slides were removed and placed back into a fresh electrolyte solution within the H-cell for electrochemical CO_2 reduction experiments. For product quantification from these aggregated films, electrochemical H-cells were first saturated with CO_2 before using an in-line Agilent 8890 GC system equipped with both a TCD and an FID. The films were irradiated at 1 sun with a Newport solar simulator (1 KW, Air Mass 1.5 Filter) throughout the electrochemical measurements or with a 390 nm P-160L Kessil LED lamp, and the products were quantified at given time points.

RESULTS AND DISCUSSION

Catalyst Attachment and Loading Levels. Initial assessment and quantification of the attachment of

https://doi.org/10.1021/acsaem.3c01670
ACS Appl. Energy Mater. 2023, 6, 10542−10553

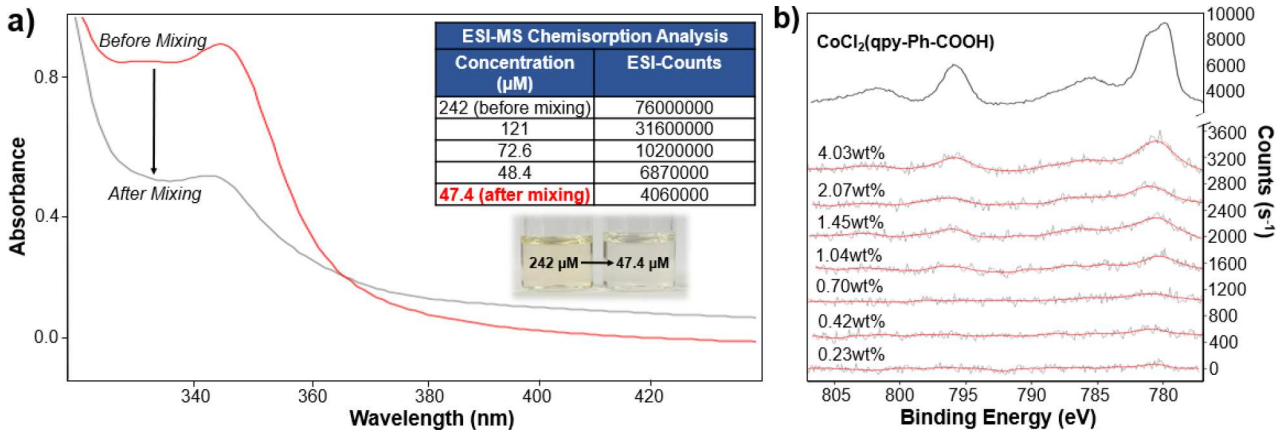

Figure 1. (a) Analysis of the $CoCl_2$(qpy-Ph-COOH) catalyst solution before and after mixing with PTI-LiCl, using UV−vis spectroscopy, ESI-MS (inset table), and a picture of the solutions' color both before and after the catalyst chemisorption (inset image) and (b) Stack plot showing the Co 2p XPS signal of the $CoCl_2$(qpy-Ph-COOH) molecular catalyst (top) and the corresponding increase in signal on the PTI-LiCl surfaces with increasing molecular catalyst wt % (bottom). The red line is a smoothing line to show signal trends more readily.

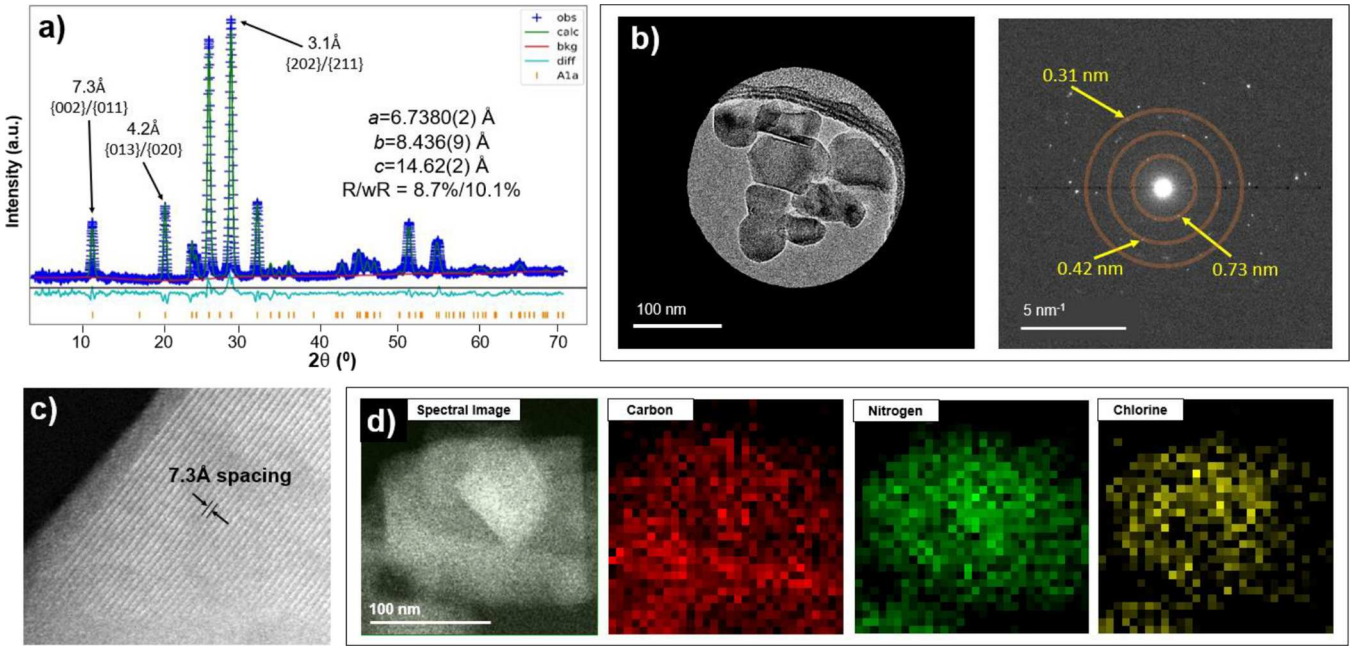

Figure 2. (a) Rietveld refinement plot of the crystalline PTI-LiCl with lattice parameters and residuals, (b) bright-field TEM image with imposed objective aperture of the hybrid $CoCl_2$(qpy-Ph-COOH)/PTI-LiCl at a 2.24 wt % catalyst loading and electron diffraction pattern, (c) lattice fringes evidenced through HAADF-STEM analysis, and (d) EDS elemental color mapping of the hybrid crystallites showing C, N, and Cl contributions.

$CoCl_2$(qpy-Ph-COOH) to PTI-LiCl were performed by using a combination of UV−vis spectroscopy and electrospray mass spectrometry (ESI-MS) of the supernatant solution after mixing and separation. A more detailed description of the procedure and methods is available in the Supporting Information. As illustrated in Figure 1a, the supernatant DMSO solution showed a significant decrease in absorbance associated with the removal of the molecular complex from solution as it attaches to the PTI-LiCl surface. The spectrum also shows that the characteristic profile of the catalyst is maintained throughout the chemisorption process with the main spectral feature occurring at $\lambda_{max} \sim 346$ nm. Owing to scattering effects in the spectra from the fine PTI-LiCl particles, ESI-MS was used for a more quantitative determination of the molar amount of attached molecular catalysts. To assess the catalyst loading, 5.5 mL of the 0.00024 M $CoCl_2$(qpy-Ph-COOH) molecular catalyst solution was mixed with 25.4 mg of PTI-LiCl (102 μmol) for an excess weight loading of 2.93 wt % (*vide infra*). The ESI-MS data of the supernatant, Figure 1a (inset), was measured to have an experimental splitting consistent with the simulated pattern and indicated the attachment of ∼1.07 μmol (83%) of catalyst from solution. This equated to 42.1 μmol of catalyst per gram of PTI-LiCl, or 2.43 wt % loaded catalyst.

The surfaces of the $CoCl_2$(qpy-Ph-COOH)/PTI-LiCl hybrid particles were characterized for increasing catalyst loadings from 0.10 to 4.03 wt %. The Co-quaterpyridine catalyst with PTI-LiCl was isolated from the solvent, ensuring that the entire amount of catalyst remained with the final dried material. XPS and FT-IR analyses were used to confirm the increasing $CoCl_2$(qpy-Ph-COOH) catalyst deposition onto the PTI-LiCl surfaces. As shown in the stack plot in Figure 1b, the

https://doi.org/10.1021/acsaem.3c01670
ACS Appl. Energy Mater. 2023, 6, 10542−10553

XPS data show an associated signal growth (bottom to top) with increasing loading of the molecular catalyst, at binding energies between 780 and 805 eV. This is consistent with the Co 2p spectral profile (upper) observed for $CoCl_2$(qpy-Ph-COOH). The XPS spectrum at the bottom shows the lowest loading, i.e., 0.23 wt %, for which a matching Co signal could yet be (barely) detected. This signal intensity increase is reflected in the Co/N and Co/Li atomic % signal ratios as shown in Table S2, with a larger ratio value corresponding to the higher weight percentages. Additionally, the carbon XPS signal (284.5 eV) and FT-IR stretch at 784 cm^{-1} were both consistent with the quaterpyridine ring and the out-of-plane ring bending mode, respectively. These signals were found to increase with increasing surface concentration of the molecular complex attached to PTI-LiCl, shown in Figures S23 and S24, thus indicating that the ligand architecture is also maintained during attachment.

Shown in Figure 2a,b are the results of the refinement of the powder X-ray diffraction data as well as electron diffraction obtained through TEM imaging of the crystalline PTI-LiCl with a 2.24 wt % catalyst loading. The structural parameters obtained from both are consistent with prior reports,[23,24] with matching reflections observed at *d*-spacing values of 7.3, 4.2, and 3.1 Å. The labeled reflections are associated with the strongly diffracting chloride anion found in the interlayer spaces of the structure, confirming that the crystallinity is maintained during the surface attachment of the catalyst. Typically, PCNs are largely characterized by the occurrence of only a single diffraction peak associated with the interlayer spacing, as observed in the high-resolution imaging of g-CN semiconductors.[25] Lattice fringes as seen in Figure 2c further confirm the crystallinity of the PTI-LiCl particles as various spacings could be identified depending on the exposed crystal facet. Low-dose EDS analyses gave excellent agreement with the elemental constituents of the PTI-LiCl semiconductor with associated EDS maps of the C, N, and Cl element components shown in Figure 2d. However, this method could not detect Co contributions stemming from the molecular catalyst at these very low surface loadings.

Light-Driven Reduction of CO_2 and Transient Absorption Spectroscopy. The obtained $CoCl_2$(qpy-Ph-COOH)/PTI-LiCl hybrid system was investigated for its photocatalytic activity for CO_2 reduction in the form of suspended powders in aqueous solution (pH ~8−9). As shown in Table 1, the initial control experiments for photocatalytic CO_2 reduction yielded appreciable rates for the hybrid material in a saturated CO_2 solution but not when purged with Ar and in the absence of $KHCO_3$. Under the latter conditions, only a small amount of H_2 is produced under irradiation, confirming that the CO product resulted from the photocatalytic CO_2 reduction and not simply degradation of the hybrid system. When the respective parts of the catalytic system were tested separately, i.e., PTI-LiCl or $CoCl_2$(qpy-Ph-COOH) alone, the production of CO is not observed. Thus, the CO_2 reduction activity is driven by electron transfer from the light-absorbing PTI, with an ~3.1 eV band gap (λ ~ 400 nm), to the $CoCl_2$(qpy-Ph-COOH) molecular catalyst. As previously described,[14,17] the molecular catalyst exhibits a high selectivity for CO_2 reduction to CO. For comparison, a more amorphous g-CN was also prepared according to previously reported procedures (Figure S31), with attachment of the molecular catalyst at 0.55 wt % loading.[14,25] However, this system failed to exhibit detectable photocatalytic activity, thus indicating a key role in the crystallinity of the PCN semiconductor.

Table 1. Control Experiments for Photocatalytic CO_2 Reduction by the $CoCl_2$(qpy-Ph-COOH)/PTI-LiCl Hybrid System Both under Ar and CO_2 and for the Catalyst and Semiconductor Components Separately[a]

sample	H_2 (μmol)	CO (μmol)	$HCOO^-$ (μmol)	net product (μmol)
Hybrid material in saturated CO_2	2.11	46.3	0	48.4
Hybrid material in Ar	11.3	0	0	11.3
PTI-LiCl	0.68	0	0.05	0.73
$CoCl_2$(qpy-Ph-COOH)	0	0	0	0

[a]Photocatalysis conditions: suspended powder (12 mg for the hybrid or PTI alone, or 4 mg in the case of the molecular catalyst alone) irradiated by a 390 nm LED lamp at 172 mW/cm^2, total time of 6 h, and sacrificial ~0.2 M Na_2SO_3 electron donor. Product analysis was collected over 5 h reaction time (after 1 h equilibration) for the gaseous headspace and over the total 6 h reaction time for the liquid solution. The control experiment for the hybrid system consisted of the $CoCl_2$(qpy-Ph-COOH) catalyst loaded at 0.55 wt % onto PTI-LiCl.

For attaining the highest rates of CO_2 reduction to CO, the optimal surface loading of the molecular catalyst onto PTI-LiCl was probed from 0.10 to 4.01 wt %. The reaction conditions were kept the same as in the above control experiments, i.e., a 390 nm LED lamp at 172 mW/cm^2 in aqueous solution. As plotted in Figure 3a, a relative plateau of activity occurs between 0.42 and 1.04 wt % of $CoCl_2$(qpy-Ph-COOH), considered here as the optimal loading range. This yielded an overall product formation rate of 1,508 μmol/g·h, with 96% CO production (1,455 μmol/g·h) at 0.42 wt %. As

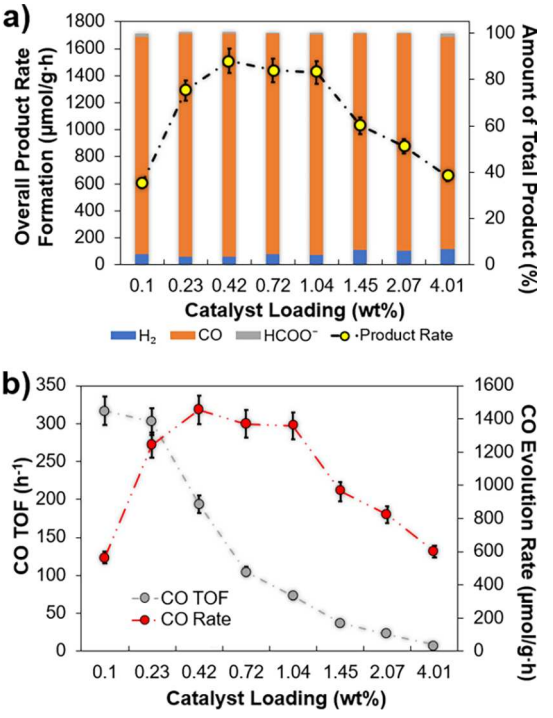

Figure 3. Photocatalysis rates and TOF as a function of the $CoCl_2$(qpy-Ph-COOH) loaded onto PTI-LiCl, plotted for (a) the product selectivity and total rates and (b) TOF for CO_2 to CO for a 4 h reaction time.

https://doi.org/10.1021/acsaem.3c01670
ACS Appl. Energy Mater. 2023, 6, 10542−10553

the loading increases incrementally from 0.42 to 1.04 wt %, the overall reduction rate remains between 1,400 and 1,550 μmol/g·h, equating to apparent quantum yields (AQY) of ~1.5 to 2.0%, as listed in the Supporting Information. At even higher loadings, a >50% drop off in the rate occurs, with a continual decrease for higher surface catalyst loadings. Notably, a maximal turnover frequency (TOF) for CO of 300+ h^{-1} is found at the lowest loadings, Figure 3b, until the 0.42 wt % threshold is reached, where it then decreases to 194 h^{-1}. This suggests that at the lowest loadings, the catalyst operates at its highest TOF for this system, with excess photogenerated electrons at each catalyst site recombining before further turnover can occur. Interestingly, at high catalyst loadings a drop in photocatalytic rates is observed. An explanation for this trend arises from the higher ratio of catalyst sites to photogenerated electrons, thus leading to lower rates of two-electron reduction products. This would be consistent with mechanistic calculations that show that the $CoCl_2$(qpy-Ph-COOH) catalyst requires two electrons for CO_2 activation.[26,27]

To further understand the kinetics of this hybrid system, transient absorption (TA) spectra were obtained on PTI films (Figure S32). Transient spectra of bare PTI-LiCl and with selected catalyst loadings of 0.13, 0.55, and 3.24 wt %, i.e., representing low, optimal, and high catalyst attachment, respectively, show a negative bleach signal in the visible region from 400 to 650 nm assigned to the stimulated emission features.[28] Photoluminescence of PTI films (Figure S34b) confirmed the broad and intense stimulated emission, which can correspond with the negative bleach signal in the TA spectra. A characteristic photoinduced absorption signal is observed at the near-IR region from 860 to 1050 nm, which has been attributed to the electron absorption of photogenerated electrons in many previous studies.[15,24,28−31] Decay kinetics of the bleach signals (Figure S33a) are found to be independent of the catalyst loading. This is consistent with a previous report in which the PL decay kinetics were found to be unaffected by the addition of electron or hole acceptors.[28] Therefore, the electron absorption signal from 900 to 920 nm was focused on to better understand the photophysics of the hybrid photocatalysts. The signal decay in this region can best be described by power law decay, $\Delta A = A_0 t^{-\beta}$ instead of simple multiexponential decay, which can be associated with trap-assisted electron−hole recombination with a broad distribution of the recombination rate constant (Figure S33b).[31] Interestingly, the electron signal decay kinetics strongly depend on the loading of the catalyst: with increasing catalyst loading from 0 to 0.55 wt %, signal decay slows down; with the catalyst loading further increased to 3.24 wt %, however, the signal decay accelerates. The change in electron signal kinetics suggests that the catalyst loading strongly modifies the electron decay pathway.

The effect of catalyst loading can be elucidated by plotting the survival probability of photogenerated electrons at a long delay time, defined as the ratio of the electron absorption signal at 300 ps to the peak amplitude, as a function of catalyst loading, as shown in Figure 4a. Although the transient signal at 300 ps has been selected for this plot, a similar trend can be observed at other delay times. Interestingly, the trend of electron survival probability versus catalyst loading agrees well with the catalyst loading dependence on the overall product rate from 0 to 0.55 wt %. This indicates that the residual signal found at a longer time scale is associated with the long-lived electron population that is responsible for the reaction. This

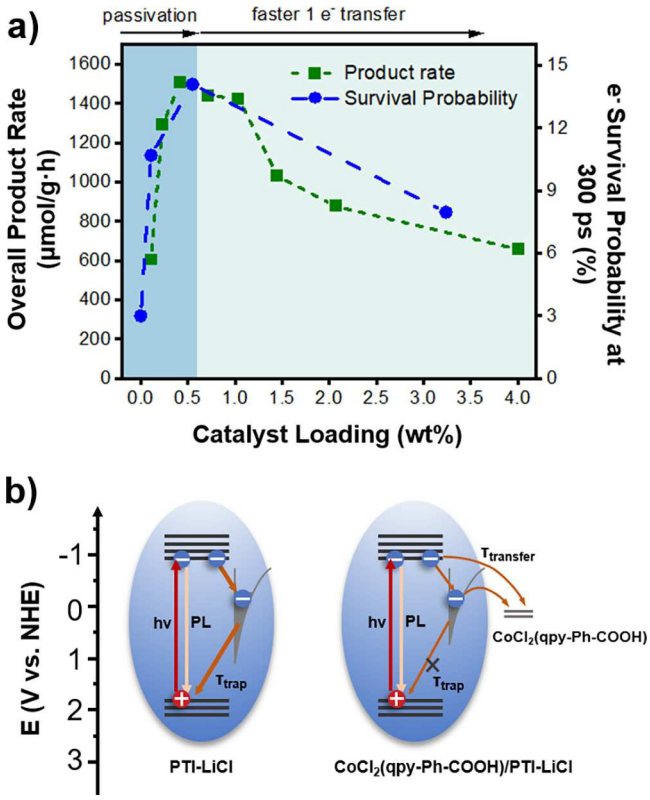

Figure 4. (a) Comparison between overall product rate trends at 172 mW/cm^2 and electron survival probability ratio at 300 ps as a function of catalyst loading. (b) Schematic for proposed charge trapping and transfer mechanism.

phenomenon likely arises from a passivation effect on the surface states, as outlined in Figure 4b. Specifically, surface defects can be passivated by the carboxylate anchoring group, slowing charge recombination and thus enabling longer-lived electrons for the chemical reaction.[32,33] The long-lived electrons will either transfer to the $CoCl_2$(qpy-Ph-COOH) catalyst directly from the conduction band or through surface-mediated charge-separated states.[34,35] As the catalyst loading increases to 3.24 wt %, the charge transfer effect dominates over the passivation effect. This results in a fast kinetic decay attributed to the electron transfer from the PTI conduction band to the Co-quaterpyridine catalyst. However, this increase in the observed electron transfer corresponds to a lower overall product generation rate. As mentioned previously, this could be attributed to a more demanding buildup of a two-electron reduced catalyst species but which is diminished by the increased concentration of one-electron reduced surface catalysts and a diluted electron concentration on PTI. The decreased generation rate of two-electron reduced catalysts will lead to a lower overall product evolution. It should be noted that the TAS measurements are not *in situ* experiments. However, competing effects of passivation and electron transfer of the catalyst should be operative as under reaction conditions, with the sacrificial donor extracting the hole and slowing the electron population decay kinetics. Thus, the TAS data provide mechanistic insights into the optimized catalyst loading region stemming from a balance between the passivation effects and the accelerated one-electron transfer. This indicates that a certain extent of electron accumulation is

https://doi.org/10.1021/acsaem.3c01670
ACS Appl. Energy Mater. 2023, 6, 10542−10553

necessary to achieve the optimum rates of two-electron CO_2 reduction.

To probe potential changes that may occur in the photocatalytic CO_2 reduction rates, the incident irradiation intensity was increased from 172 to 260 mW/cm^2 (51% intensity increase) for the catalyst loadings between 0.10 and 1.45 wt %. These catalyst loadings were selected to probe the impact on the CO production rates below (0.10 and 0.23 wt %), at (0.42−1.04 wt %), and above (1.45 wt %) the optimal loading amounts. As shown in Figure 5a, at the lower catalyst

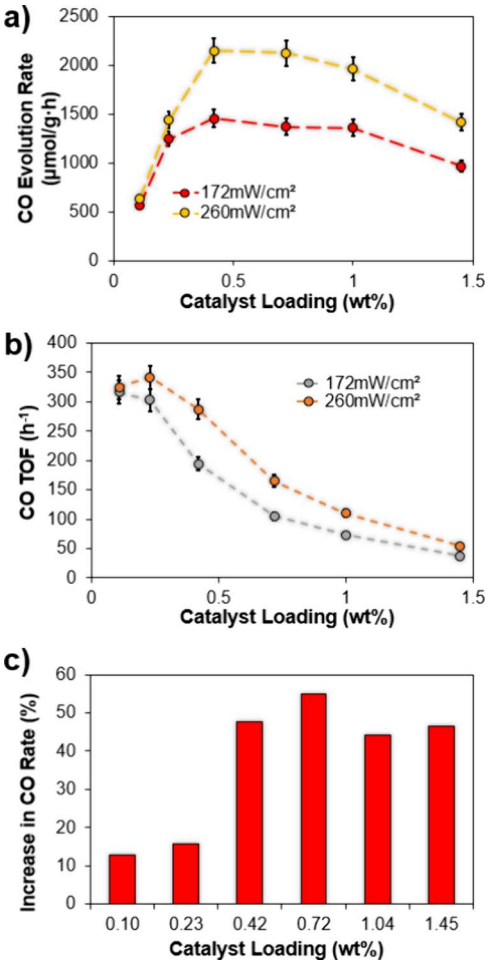

Figure 5. Photocatalytic performance at weight loadings from 0.10 to 1.45 wt % for two light irradiances, as shown plotted together for the (a) CO production rate, (b) TOF, and (c) percent increase in the CO rate when increasing the light irradiance.

loadings, i.e., 0.10 and 0.23 wt %, there is an almost negligible increase in CO production rates owing to the catalyst sites already operating at their maximal TOF under the lower light intensity. At these loadings, the AQY also decreases by ∼29−30% at the higher irradiance, as shown in Table S2 in the Supporting Information. Conversely, there is a clear increase in the CO rates for catalyst loadings of ≥0.42 wt % at higher irradiance. For example, the optimally loaded catalyst at 0.42 wt % shows the highest attained rate of 2,149 μmol CO/g·h with 96% product selectivity, corresponding to a TOF increase from 194 to 287 h^{-1} (Figure 5a,b). This approaches the maximal TOF observed at the lower catalyst loadings (∼330 h^{-1} at 260 mW/cm^2). As shown in Figure 5c, the percent increase in CO production rates at the higher catalyst loadings of ≥0.42 wt %, i.e., 47.4%, matches the percentage increase in incident photons from 172 to 260 mW/cm^2 of ∼51%. This is consistent with a direct conversion of additional photons to higher CO_2 reduction rates, with the associated AQY values decreasing by a much smaller ∼6 to 12%. The remainder of the total product can be attributed to the co-evolved H_2 and $HCOO^-$ (≈4−5%). This suggests that higher rates of CO_2 reduction to CO can be achieved using more concentrated light sources and higher catalyst loadings rather than being limited by charge-carrier recombination rates in the crystalline PTI-LiCl. An increased diffusion rate of excited electrons reaching the surfaces can drive a greater number of two-electron reduced catalyst sites, thus effectively initiating the CO_2 coordination and reduction steps to give CO.

The photocatalytic stability of the $CoCl_2$(qpy-Ph-COOH)/PTI-LiCl hybrid was probed via extended reaction times of up to 32 h, as shown in Figure 6. The rate of CO production was

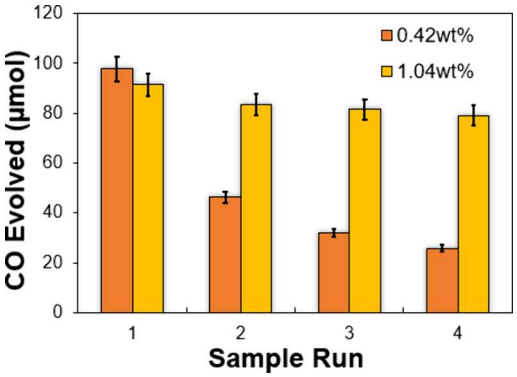

Figure 6. Plot of CO evolution for long-term testing at two different catalyst loadings, 0.42 and 1.04 wt %, with four consecutive sample runs and measured gas evolved over 7 h.

tested over the course of four consecutive runs, with each time reusing the same sample and reaction solution. At the 0.42 wt % loading, there is a dropoff in the CO production rate over consecutive experiments, with run 4 yielding only 26.5% of the original CO rate. This deactivation with time has been observed with other molecular catalysts and is found to typically result from the detachment of the metal cation from the ligand and surfaces.[15] Interestingly, by increasing the catalyst loading on the surface to 1.04 wt %, a mitigation of the catalyst deactivation was observed. At this higher loading, the hybrid material maintains a much higher 86.5% of its initial activity after 32 h, with a production rate of 1,012 μmol CO/g·h over the last 8 h reaction period. A measured 30,000+ μmol CO/g over the course of the 28 h was quantified. This behavior likely arises from the plateau in activity previously found between 0.42 and 1.0 wt % (Figure 4a). Catalyst deactivation and thus the slowing in the rate of CO production can be offset by an increase in TOF of the remaining operative catalyst sites as the reaction proceeds. At higher loadings, the excess $CoCl_2$(qpy-Ph-COOH) surface sites have the built-in capacity to be driven at higher TOFs to maintain the overall rate. These results demonstrate that increased irradiance levels and excess surface catalysts can be utilized as potential strategies for addressing rate limitations and deactivation pathways that have been described in prior PCN studies.[15,29]

By comparison to more amorphous g-CN materials, the hybrid $CoCl_2$(qpy-Ph-COOH)/PTI-LiCl catalyst system exhibits significantly higher rates of photocatalytic CO

https://doi.org/10.1021/acsaem.3c01670
ACS Appl. Energy Mater. 2023, 6, 10542−10553

production in aqueous solutions while maintaining a high selectivity. A comparative plot of photocatalytic CO rates and selectivity from relevant literature reports is illustrated in Figure 7. This plot reveals that the $CoCl_2$(qpy-Ph-COOH)/PTI-LiCl hybrid exhibits rates exceeding those in prior reports in per mass of photocatalyst.[12,15,36−43,44] Most notably, this hybrid catalyst functions in aqueous solution as compared to prior studies reporting rates for photocatalytic CO_2 reduction in predominantly organic solvents. The only prior study involving a PCN semiconductor with >500 μmol CO/g·h in a partly aqueous-based solution (1:2 ratio of water with acetonitrile) reported ~637 μmol CO/g·h using C_xN_y nanosheets in combination with $ZnIn_2S_4$.[41] This rate is labeled by a star in Figure 7, showing <30% of the comparable CO production activity as found herein, as labeled by the green and red diamonds. The superior photocatalytic rates of the $CoCl_2$(qpy-Ph-COOH)/PTI-LiCl hybrid stem from the crystallinity of the PTI-LiCl semiconductor and the capability of the molecular catalyst to effectively passivate its surface defects. These effects help to minimize both bulk-mediated and surface-mediated recombination, enabling more efficient electron diffusion to the surface catalysts and the higher reduction rates and TOFs.

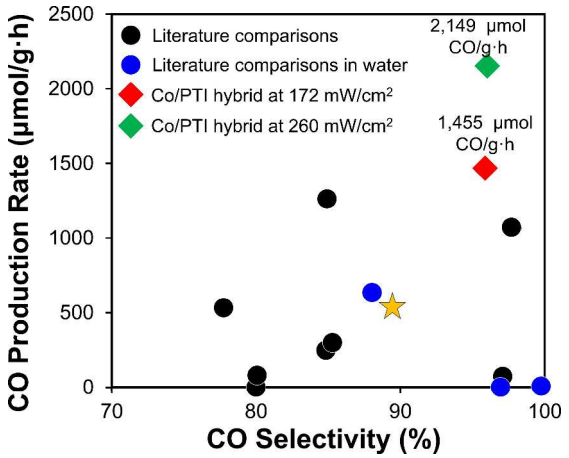

Figure 7. Comparison of photocatalysis rates of carbon-nitride based hybrid particles for CO_2 reduction to CO, showing the superior activity and selectivity of $CoCl_2$(qpy-Ph-COOH)/PTI-LiCl as compared to other carbon-nitride based systems. Tabulated values and references are listed in the Supporting Information.

Catalytic CO_2 Reduction of Deposited Hybrid Particles. A low-bias electrophoretic deposition technique was used to deposit the hybrid $CoCl_2$(qpy-Ph-COOH)/PTI-LiCl particles onto conductive FTO slides,[45] with the aim to eliminate the need for sacrificial reagents as well as to probe the impact of an electrochemical bias on its photocatalytic activity. As pictured in Figure 8a, a film of the hybrid particles was deposited from an aqueous suspension at an applied bias of −1.2 V vs Ag/AgCl. At this potential, deposition of the hybrid catalyst particles onto the FTO substrate required the starting suspended PTI-LiCl powder to have a high loading of the $CoCl_2$(qpy-Ph-COOH) catalyst (~4.30 wt % in this case). The particle film was sufficiently robust and could be removed and placed back into a fresh electrolyte without observable degradation or delamination. Characterization of the films by FT-IR, shown in Figure 8b, revealed absorption peaks associated with PTI-LiCl together with $KHCO_3$ from the dried aqueous solution. The SEM images of the hybrid particles and associated EDS analysis, Figure 8c−e, further confirmed the deposition of aggregates of the hybrid $CoCl_2$(qpy-Ph-COOH)/PTI-LiCl particles.

Next, the photocatalytic activity and CO_2 reduction products of the deposited hybrid particles were investigated in an aqueous 0.5 M $KHCO_3$ solution under an applied bias and without sacrificial reagents. These reactions were performed in the cathodic compartment of an H-cell, as

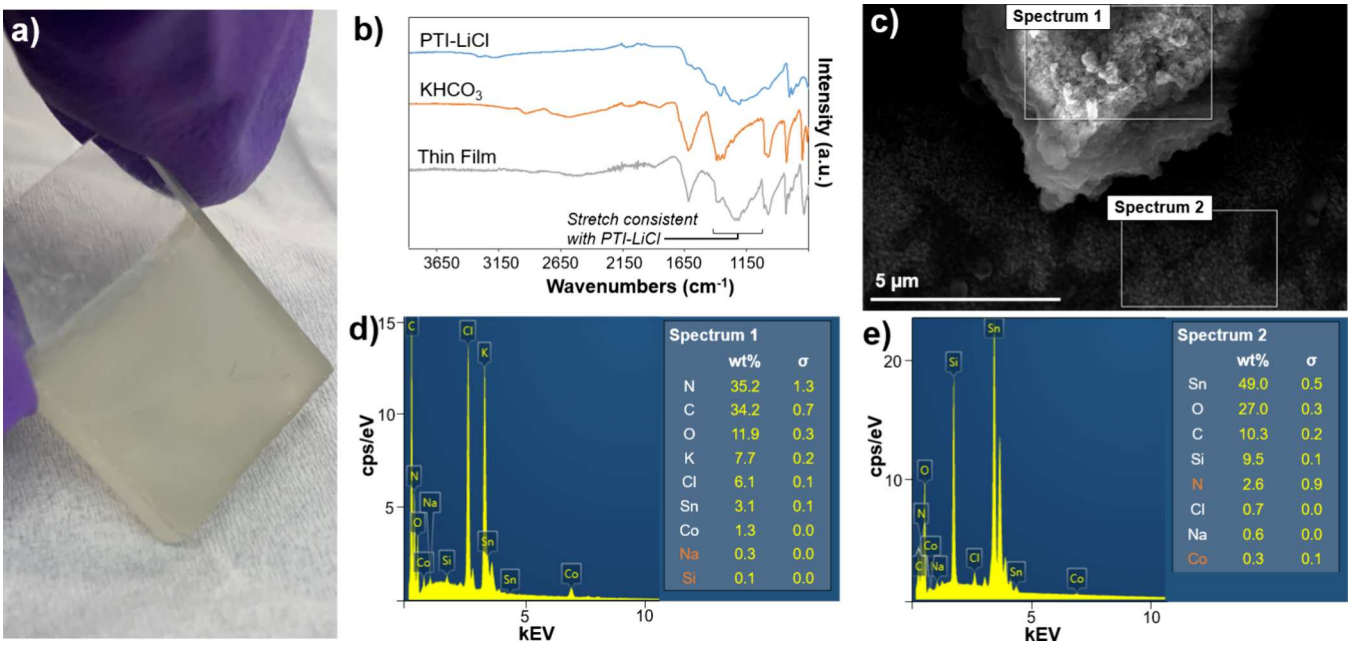

Figure 8. Deposition of hybrid particles, showing (a) an optical image of the resulting film, (b) FTIR analysis showing stretches consistent with PTI-LiCl on the surface, (c) SEM image of the hybrid material on the FTO surface, and (d, e) EDS analyses for the FTO substrate with and without hybrid particles, respectively.

https://doi.org/10.1021/acsaem.3c01670
ACS Appl. Energy Mater. 2023, 6, 10542−10553

Table 2. Photocatalytic CO_2 Reduction under Applied Bias for Particle-Deposited Films of $CoCl_2$(qpy-Ph-COOH)/PTI-LiCl over the Course of 1 h with Products and Faradaic Efficiencies[a]

sample	E vs Ag/AgCl	FE for H_2 (%)	H_2 (μmol)	FE for CO (%)	CO (μmol)	total gaseous FE (%)	net charge (C)
sample 1	−0.8 V	9.81	0.025	5.89	0.015	15.7	0.05
sample 2	−1.2 V	19.1	1.17	60.5	3.70	79.6	1.18
sample 3	−1.6 V	47.7	36.6	17.7	13.6	65.4	14.8
FTO blank	−1.2 V	30.24	0.57	5.26	0.10	35.5	0.37

[a]Reaction conditions: Aqueous 0.5 M $KHCO_3$ (pH ∼8−9) solution purged with CO_2(g) until saturation; irradiated at 1 sun (100 mW/cm^2) with a Newport solar simulator with a 0.5 cm^2 irradiation window; hybrid particles were prepared from PTI-LiCl with the $CoCl_2$(qpy-Ph-COOH) catalyst loaded at 4.30 wt %. FE and net charge values represent the time between 0.5 and 1.5 h of the potential hold in which products were quantified.

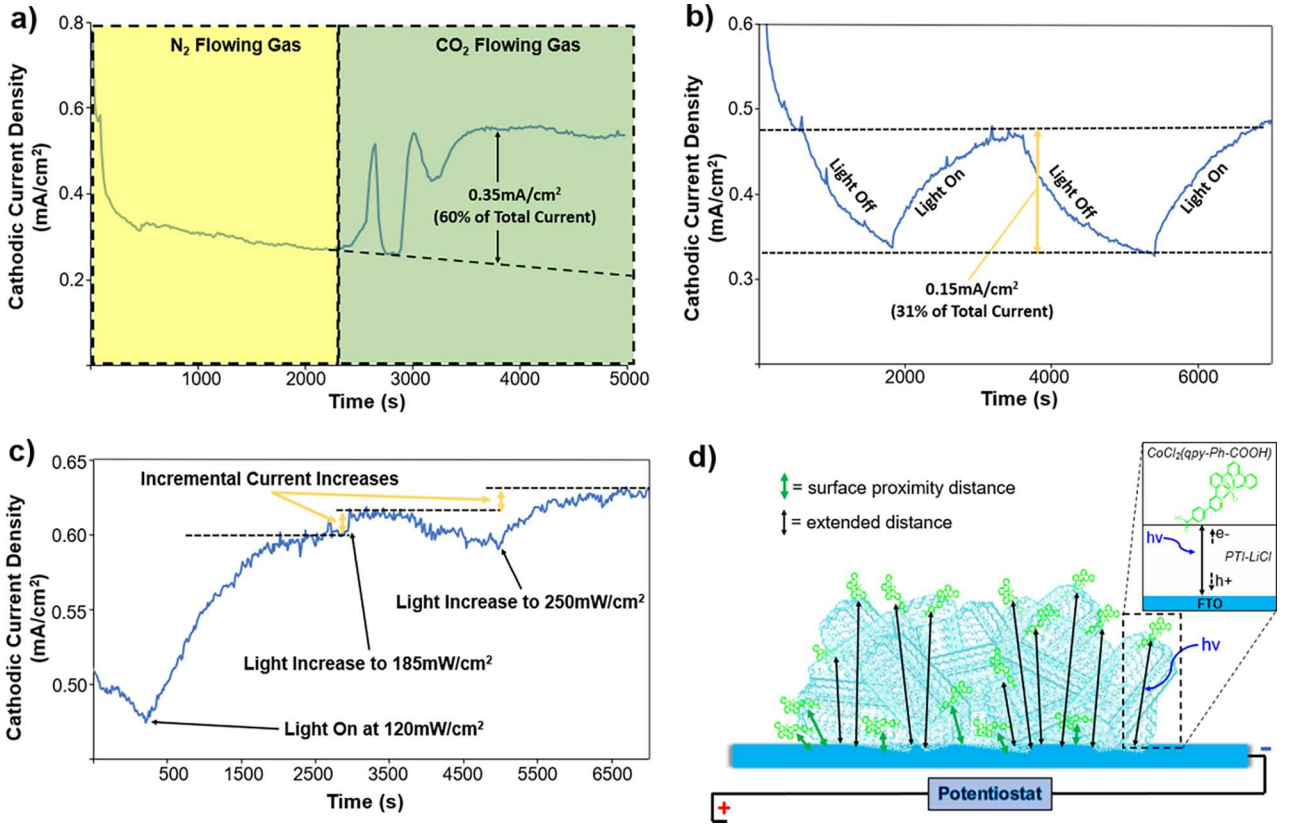

Figure 9. Photocathodic current density (390 nm; 172 mW/cm^2) of particle-deposited hybrid films under an applied bias (−1.2 V vs Ag/AgCl), showing the impact of (a) flowing N_2 (yellow) and CO_2 (green) in an aqueous 0.5 M $KHCO_3$ solution, (b) alternating dark vs light irradiation, (c) stepwise increasing irradiance, and (d) schematic of the aggregated particle film and energy schematic.

described in the Experimental Section, at applied biases of −0.8, −1.2, and −1.6 V vs Ag/AgCl. Initial cyclic voltammograms were used to select these three applied biases for the characterization of the product distribution, as notated in Figure S38a. At an applied bias of −1.2 V, a stable cathodic current density of ∼0.7 mA·cm^{-2} was measured over the course of 1.5 h. As tabulated in Table 2, the highest Faradaic efficiency (FE) was also obtained for the reduction of CO_2 to CO at −1.2 V, in which a 60% FE for CO as well as up to 80% FE for the total gaseous products was observed. When compared to a bare FTO glass slide, ≥97% of the evolved CO can be attributed to the deposited hybrid particles. At the more negative applied bias of −1.6 V, while the amount of CO produced increases, i.e., from 7.2 to 27.2 μmol/cm^2·h, the FE drops significantly to 17.7%. This arises because H_2 evolution predominates at a more negative applied bias. The formation of $HCOO^-$ could not be detected using NMR spectroscopy.

Control experiments were performed to probe the origin of the cathodic currents of the deposited hybrid particles. The films were inserted into an H-cell with flowing gas and incident irradiation from a 390 nm LED light source. As the purging gas was switched from N_2 to CO_2, Figure 9a, the measured cathodic currents showed an increase of ∼0.35 mA/cm^2 that was associated with the preference for CO_2 reduction at −1.2 V vs Ag/AgCl. This boost in the cathodic current eventually equilibrates with the saturation of the flowing CO_2. Even though not intimately sintered onto the FTO substrate, the deposited hybrid aggregates show light-driven cathodic currents of ∼0.15 mA/cm^2 when under irradiation as compared to under dark conditions under flowing CO_2. However, the stepwise changes in the cathodic current density with alternating dark/light irradiation, Figure 9b, showed a relatively slow response on the order of 30 min. This suggests that a slow reorganization of the deposited particles on the substrate occurs under light irradiation. While effects from the

https://doi.org/10.1021/acsaem.3c01670
ACS Appl. Energy Mater. 2023, 6, 10542−10553

FTO surface should be considered, control studies with bare FTO show comparably very low to negligible photocurrent densities by itself. As shown in Figure 9c, there is a large initial increase with incident light irradiation and further intensity increases resulting in incrementally growing current densities. These observations are consistent with an appreciable dark current arising from molecular catalysts that are in close proximity to the conducting FTO surface (or on it), with the light-driven response arising from molecular catalysts attached to the hybrid aggregates at a farther distance from the substrate, as illustrated in Figure 9d. The FE for CO production was also probed in the dark versus under light irradiation, showing a FE increase for CO production from 38.4 to 57.5% (Figure S39 and Table S11) and confirming the light-driven origin of the increased CO production. Future improvements in design and efficiency could potentially be achieved by the development of more uniform and organized catalyst/PCN films, such as by increasing the particle film coverage, attaining more intimate contact to the substrate, and placement of the molecular catalysts away from the conducting substrate to minimize the dark current.

CONCLUSIONS

A new semiconductor/molecular catalyst hybrid system for light-driven CO_2 reduction in aqueous solution has been discovered based on the efficacious attachment of a $CoCl_2$(qpy-Ph-COOH) molecular catalyst to a crystalline carbon nitride, PTI-LiCl. Characterization of this hybrid system by UV−vis, ESI-MS, and XPS techniques showed a relatively narrow optimal range for catalyst loading of ∼0.42 to 1.04 wt %. The optimized photocatalytic rates for CO_2 reduction are found at 0.42 wt % of $CoCl_2$(qpy-Ph-COOH), with a CO production rate of 2,149 μmol CO/g·h, a TOF of 287 h^{-1}, and AQY of ∼1.5 to 2.0% under 260 mW/cm^2 irradiation at 390 nm. The obtained photocatalytic rates and apparent optimal quantum yields represent among the highest currently reported for suspended particle photocatalysis with the use of carbon nitride semiconductors. TAS results indicate a mechanism consistent with passivation of surface defects arising from the attachment of the molecular catalysts via their −COOH groups onto the PTI-LiCl particles, thus decreasing the electron−hole recombination rates. At higher loadings, a fast one-electron reduction of the surface catalysts can be observed which leads to a diluted electron concentration on PTI. This, in turn, inhibits the buildup of two-electrons per catalyst site required to drive CO_2 coordination and reduction by the $CoCl_2$(qpy-Ph-COOH) molecular catalyst. However, higher CO production rates and longer catalyst stability can be achieved with excess loading of molecular catalysts onto the PTI-LiCl surfaces. This stems from a greater built-in catalyst capacity for utilizing higher rates of excited electrons or to help offset catalyst deactivation with time. The hybrid particles can also be electrophoretically deposited as an aggregated film onto a conductive FTO substrate and exhibit an FE for CO production of ∼60% at −1.2 V vs Ag/AgCl under 1 sun irradiation. Thus, these results demonstrate a successful new approach for synergistically combining a crystalline carbon nitride with a molecular catalyst, which function together to achieve among the highest known rates and AQY (for carbon-nitride based systems) for the light-driven reduction of CO_2 to CO in aqueous solution with >95% selectivity.

ASSOCIATED CONTENT

Supporting Information

The Supporting Information is available free of charge at https://pubs.acs.org/doi/10.1021/acsaem.3c01670.

Detailed experimental procedures pertaining to synthesis and photocatalysis reactions, product characterization by NMR, powder XRD, XPS, FT-IR, SEM, GC, and ESI-MS, pictures of photocatalysis and photoelectrochemical setups with associated calibration curves and calculations for quantification of products, rates and AQY, procedures and data for transient absorption spectroscopy measurements and analysis, table of literature comparisons for carbon nitride-based systems for CO_2 reduction with associated references, and pictures and data analyses for electrophoretic deposition of hybrid particles and their photoelectrochemical testing (PDF)

AUTHOR INFORMATION

Corresponding Author

Paul A. Maggard − *Department of Chemistry, North Carolina State University, Raleigh, North Carolina 27695, United States;* orcid.org/0000-0002-3909-1590; Email: Paul_Maggard@ncsu.edu

Authors

Scott McGuigan − *Department of Chemistry, North Carolina State University, Raleigh, North Carolina 27695, United States;* orcid.org/0000-0002-9554-0151

Stephen J. Tereniak − *Department of Chemistry, University of North Carolina at Chapel Hill, Chapel Hill, North Carolina 27599, United States*

Carrie L. Donley − *Department of Chemistry, University of North Carolina at Chapel Hill, Chapel Hill, North Carolina 27599, United States;* orcid.org/0000-0003-0906-306X

Avery Smith − *Department of Chemistry, North Carolina State University, Raleigh, North Carolina 27695, United States*

Sungho Jeon − *Department of Materials Science and Engineering, University of Pennsylvania, Philadelphia, Pennsylvania 19104, United States*

Fengyi Zhao − *Department of Chemistry, Emory University, Atlanta, Georgia 30322, United States;* orcid.org/0000-0003-4837-9294

Renato N. Sampaio − *Department of Chemistry, University of North Carolina at Chapel Hill, Chapel Hill, North Carolina 27599, United States;* orcid.org/0000-0002-7158-6470

Magnus Pauly − *Department of Chemistry, North Carolina State University, Raleigh, North Carolina 27695, United States*

Landon Keller − *Department of Chemical Engineering, North Carolina State University, Raleigh, North Carolina 27695, United States*

Leonard Collins − *Molecular Education, Technology and Research Innovation Center (METRIC), North Carolina State University, Raleigh, North Carolina 27695, United States*

Gregory N. Parsons − *Department of Chemical Engineering, North Carolina State University, Raleigh, North Carolina 27695, United States;* orcid.org/0000-0002-0048-5859

Tianquan Lian − *Department of Chemistry, Emory University, Atlanta, Georgia 30322, United States;* orcid.org/0000-0002-8351-3690

https://doi.org/10.1021/acsaem.3c01670
ACS Appl. Energy Mater. 2023, 6, 10542−10553

Eric A. Stach − *Department of Materials Science and Engineering, University of Pennsylvania, Philadelphia, Pennsylvania 19104, United States;* orcid.org/0000-0002-3366-2153

Complete contact information is available at: https://pubs.acs.org/10.1021/acsaem.3c01670

Notes

The authors declare no competing financial interest.

■ ACKNOWLEDGMENTS

This work was entirely supported as part of the Center for Hybrid Approaches in Solar Energy to Liquid Fuels (CHASE), an Energy Innovation Hub funded by the U.S. Department of Energy, Office of Science, Office of Basic Energy Sciences under Award Number DE-SC0021173. Research efforts were performed in part at the Molecular Education, Technology and Research Innovation Center (METRIC) at NC State University, and at the University of North Carolina's Chapel Hill Analytical and Nanofabrication Laboratory, CHANL, a member of the North Carolina Research Triangle Nanotechnology Network, RTNN, which is supported by the National Science Foundation, Grant ECCS-2025064, as part of the National Nanotechnology Coordinated Infrastructure, NNCI. The authors thank the University of North Carolina's Department of Chemistry NMR Core Laboratory for the use of their NMR spectrometers, particularly the instrument funded under the National Science Foundation Grant No. CHE-1828183. The authors thank the University of North Carolina's Department of Chemistry Mass Spectrometry Core Laboratory for the use of their mass spectrometer funded by the National Science Foundation under Grant No. CHE-1726291. The S/TEM analysis was carried out at the Singh Center for Nanotechnology, which is supported by the NSF National Nanotechnology Coordinated Infrastructure Program under grant NNCI-2025608 and Laboratory for Research on the Structure of Matter (MRSEC) supported by the National Science Foundation (DMR-1720530).

■ REFERENCES

(1) Solomon, S.; Plattner, G.-K.; Knutti, R.; Friedlingstein, P. Irreversible Climate Change Due to Carbon Dioxide Emissions. *Proc. Natl. Acad. Sci. U. S. A.* **2009**, *106* (6), 1704−1709.

(2) Lewis, N. S.; Nocera, D. G. Powering the Planet: Chemical Challenges in Solar Energy Utilization. *Proc. Natl. Acad. Sci. U. S. A.* **2006**, *103* (43), 15729−15735.

(3) Reyes Cruz, E. A.; Nishiori, D.; Wadsworth, B. L.; Nguyen, N. P.; Hensleigh, L. K.; Khusnutdinova, D.; Beiler, A. M.; Moore, G. F. Molecular-Modified Photocathodes for Applications in Artificial Photosynthesis and Solar-to-Fuel Technologies. *Chem. Rev.* **2022**, *122* (21), 16051−16109.

(4) Rajeshwar, K.; Maggard, P. A.; O'Donnell, S. In Search of the "Perfect" Inorganic Semiconductor/Liquid Interface for Solar Water Splitting. *Electrochem. Soc. Interface* **2021**, *30* (1), 47.

(5) Thangamuthu, M.; Ruan, Q.; Ohemeng, P. O.; Luo, B.; Jing, D.; Godin, R.; Tang, J. Polymer Photoelectrodes for Solar Fuel Production: Progress and Challenges. *Chem. Rev.* **2022**, *122* (13), 11778−11829.

(6) Banerjee, T.; Podjaski, F.; Kröger, J.; Biswal, B. P.; Lotsch, B. V. Polymer Photocatalysts for Solar-to-Chemical Energy Conversion. *Nat. Rev. Mater.* **2021**, *6* (2), 168−190.

(7) Kessler, F. K.; Zheng, Y.; Schwarz, D.; Merschjann, C.; Schnick, W.; Wang, X.; Bojdys, M. J. Functional Carbon Nitride Materials — Design Strategies for Electrochemical Devices. *Nat. Rev. Mater.* **2017**, *2* (6), 17030 DOI: 10.1038/natrevmats.2017.30.

(8) Lin, J.; Tian, W.; Zhang, H.; Duan, X.; Sun, H.; Wang, S. Graphitic Carbon Nitride-Based Z-Scheme Structure for Photocatalytic CO_2 Reduction. *Energy Fuels* **2021**, *35* (1), 7−24.

(9) Liu, M.; Wei, C.; Zhuzhang, H.; Zhou, J.; Pan, Z.; Lin, W.; Yu, Z.; Zhang, G.; Wang, X. Fully Condensed Poly (Triazine Imide) Crystals: Extended π-Conjugation and Structural Defects for Overall Water Splitting. *Angew. Chem., Int. Ed.* **2022**, *61* (2), No. e202113389, DOI: 10.1002/anie.202113389.

(10) Nakada, A.; Kumagai, H.; Robert, M.; Ishitani, O.; Maeda, K. Molecule/Semiconductor Hybrid Materials for Visible-Light CO_2 Reduction: Design Principles and Interfacial Engineering. *Accounts Mater. Res.* **2021**, *2* (6), 458−470.

(11) Maeda, K.; Sekizawa, K.; Ishitani, O. A Polymeric-Semiconductor−Metal-Complex Hybrid Photocatalyst for Visible-Light CO_2 Reduction. *Chem. Commun.* **2013**, *49* (86), 10127−10129.

(12) Cometto, C.; Kuriki, R.; Chen, L.; Maeda, K.; Lau, T.-C.; Ishitani, O.; Robert, M. A Carbon Nitride/Fe Quaterpyridine Catalytic System for Photostimulated CO_2-to-CO Conversion with Visible Light. *J. Am. Chem. Soc.* **2018**, *140* (24), 7437−7440.

(13) Wei, Y.; Chen, L.; Chen, H.; Cai, L.; Tan, G.; Qiu, Y.; Xiang, Q.; Chen, G.; Lau, T.; Robert, M. Highly Efficient Photocatalytic Reduction of CO_2 to CO by in Situ Formation of a Hybrid Catalytic System Based on Molecular Iron Quaterpyridine Covalently Linked to Carbon Nitride. *Angew. Chem., Int. Ed.* **2022**, *61* (11), No. e202116832, DOI: 10.1002/ange.202116832.

(14) Ma, B.; Chen, G.; Fave, C.; Chen, L.; Kuriki, R.; Maeda, K.; Ishitani, O.; Lau, T.-C.; Bonin, J.; Robert, M. Efficient Visible-Light-Driven CO_2 Reduction by a Cobalt Molecular Catalyst Covalently Linked to Mesoporous Carbon Nitride. *J. Am. Chem. Soc.* **2020**, *142* (13), 6188−6195.

(15) Shang, B.; Zhao, F.; Choi, C.; Jia, X.; Pauly, M.; Wu, Y.; Tao, Z.; Zhong, Y.; Harmon, N.; Maggard, P. A.; Lian, T.; Hazari, N.; Wang, H. Monolayer Molecular Functionalization Enabled by Acid−Base Interaction for High-Performance Photochemical CO_2 Reduction. *ACS Energy Lett.* **2022**, *7* (7), 2265−2272.

(16) Ma, X.; Hu, C.; Bian, Z. Hybrid Photocatalytic Systems Comprising a Manganese Complex Anchored on G-C3N4 for Efficient Visible-Light Photoreduction of CO_2. *Inorg. Chem. Commun.* **2020**, *117*, No. 107951.

(17) Wang, M.; Chen, L.; Lau, T.; Robert, M. A Hybrid Co Quaterpyridine Complex/Carbon Nanotube Catalytic Material for CO_2 Reduction in Water. *Angew. Chemie Int. Ed.* **2018**, *57* (26), 7769−7773.

(18) Cometto, C.; Chen, L.; Lo, P.-K.; Guo, Z.; Lau, K.-C.; Anxolabéhère-Mallart, E.; Fave, C.; Lau, T.-C.; Robert, M. Highly Selective Molecular Catalysts for the CO_2-to-CO Electrochemical Conversion at Very Low Overpotential. Contrasting Fe vs Co Quaterpyridine Complexes upon Mechanistic Studies. *ACS Catal.* **2018**, *8* (4), 3411−3417.

(19) Yang, P.; Zhao, J.; Qiao, W.; Li, L.; Zhu, Z. Ammonia-Induced Robust Photocatalytic Hydrogen Evolution of Graphitic Carbon Nitride. *Nanoscale* **2015**, *7* (45), 18887−18890.

(20) Cao, S.; Low, J.; Yu, J.; Jaroniec, M. Polymeric Photocatalysts Based on Graphitic Carbon Nitride. *Adv. Mater.* **2015**, *27* (13), 2150−2176.

(21) Wirnhier, E.; Döblinger, M.; Gunzelmann, D.; Senker, J.; Lotsch, B. V.; Schnick, W. Poly(Triazine Imide) with Intercalation of Lithium and Chloride Ions $[(C_3N_3)_2(NH_xLi_{1-x})_3{\cdot}LiCl]$: A Crystalline 2D Carbon Nitride Network. *Chem. − Eur. J.* **2011**, *17* (11), 3213−3221, DOI: 10.1002/chem.201002462.

(22) Mesch, M. B.; Bärwinkel, K.; Krysiak, Y.; Martineau, C.; Taulelle, F.; Neder, R. B.; Kolb, U.; Senker, J. Solving the Hydrogen and Lithium Substructure of Poly (Triazine Imide)/LiCl Using NMR Crystallography. *Chem.—Eur. J.* **2016**, *22* (47), 16878−16890, DOI: 10.1002/chem.201603726.

(23) Pauly, M.; Kröger, J.; Duppel, V.; Murphey, C.; Cahoon, J.; Lotsch, B. V.; Maggard, P. A. Unveiling the Complex Configurational

Landscape of the Intralayer Cavities in a Crystalline Carbon Nitride. *Chem. Sci.* **2022**, *13* (11), 3187−3193.
(24) Liu, M.; Zhang, G.; Liang, X.; Pan, Z.; Zheng, D.; Wang, S.; Yu, Z.; Hou, Y.; Wang, X. Rh/Cr_2O_3 and CoO_x Cocatalysts for Efficient Photocatalytic Water Splitting by Poly (Triazine Imide) Crystals. *Angew. Chem.* **2023**, *135* (37), No. e202304694, DOI: 10.1002/ange.202304694.
(25) Wang, A.; Wang, C.; Fu, L.; Wong-Ng, W.; Lan, Y. Recent Advances of Graphitic Carbon Nitride-Based Structures and Applications in Catalyst, Sensing, Imaging, and LEDs. *Nano-Micro Lett.* **2017**, *9*, 1−21, DOI: 10.1007/s40820-017-0148-2.
(26) Loipersberger, M.; Cabral, D. G. A.; Chu, D. B. K.; Head-Gordon, M. Mechanistic Insights into Co and Fe Quaterpyridine-Based CO_2 Reduction Catalysts: Metal−Ligand Orbital Interaction as the Key Driving Force for Distinct Pathways. *J. Am. Chem. Soc.* **2021**, *143* (2), 744−763.
(27) Guo, Z.; Cheng, S.; Cometto, C.; Anxolabéhère-Mallart, E.; Ng, S.-M.; Ko, C.-C.; Liu, G.; Chen, L.; Robert, M.; Lau, T.-C. Highly Efficient and Selective Photocatalytic CO_2 Reduction by Iron and Cobalt Quaterpyridine Complexes. *J. Am. Chem. Soc.* **2016**, *138* (30), 9413−9416.
(28) Corp, K. L.; Schlenker, C. W. Ultrafast Spectroscopy Reveals Electron-Transfer Cascade That Improves Hydrogen Evolution with Carbon Nitride Photocatalysts. *J. Am. Chem. Soc.* **2017**, *139* (23), 7904−7912.
(29) Yang, W.; Godin, R.; Kasap, H.; Moss, B.; Dong, Y.; Hillman, S. A. J.; Steier, L.; Reisner, E.; Durrant, J. R. Electron Accumulation Induces Efficiency Bottleneck for Hydrogen Production in Carbon Nitride Photocatalysts. *J. Am. Chem. Soc.* **2019**, *141* (28), 11219−11229.
(30) Khan, M. A.; Maity, P.; Al-Oufi, M.; Al-Howaish, I. K.; Idriss, H. Electron Transfer of the Metal/Semiconductor System in Photocatalysis. *J. Phys. Chem. C* **2018**, *122* (29), 16779−16787.
(31) Godin, R.; Wang, Y.; Zwijnenburg, M. A.; Tang, J.; Durrant, J. R. Time-Resolved Spectroscopic Investigation of Charge Trapping in Carbon Nitrides Photocatalysts for Hydrogen Generation. *J. Am. Chem. Soc.* **2017**, *139* (14), 5216−5224.
(32) Hara, K.; Dan-oh, Y.; Kasada, C.; Ohga, Y.; Shinpo, A.; Suga, S.; Sayama, K.; Arakawa, H. Effect of Additives on the Photovoltaic Performance of Coumarin-Dye-Sensitized Nanocrystalline TiO_2 Solar Cells. *Langmuir* **2004**, *20* (10), 4205−4210.
(33) Wang, P.; Zakeeruddin, S. M.; Humphry-Baker, R.; Moser, J. E.; Grätzel, M. Molecular-scale Interface Engineering of TiO_2 Nanocrystals: Improve the Efficiency and Stability of Dye-sensitized Solar Cells. *Adv. Mater.* **2003**, *15* (24), 2101−2104.
(34) Xue, J.; Fujitsuka, M.; Majima, T. Shallow Trap State-Enhanced Photocatalytic Hydrogen Evolution over Thermal-Decomposed Polymeric Carbon Nitride. *Chem. Commun.* **2020**, *56* (44), 5921−5924.
(35) Xue, J.; Fujitsuka, M.; Majima, T. Near Bandgap Excitation Inhibits the Interfacial Electron Transfer of Semiconductor/Cocatalyst. *ACS Appl. Mater. Interfaces* **2020**, *12* (5), 5920−5924.
(36) Lin, L.; Lin, Z.; Zhang, J.; Cai, X.; Lin, W.; Yu, Z.; Wang, X. Molecular-Level Insights on the Reactive Facet of Carbon Nitride Single Crystals Photocatalysing Overall Water Splitting. *Nat. Catal.* **2020**, *3* (8), 649−655.
(37) Qin, J.; Wang, S.; Ren, H.; Hou, Y.; Wang, X. Photocatalytic Reduction of CO_2 by Graphitic Carbon Nitride Polymers Derived from Urea and Barbituric Acid. *Appl. Catal. B Environ.* **2015**, *179*, 1−8.
(38) Zhao, G.; Pang, H.; Liu, G.; Li, P.; Liu, H.; Zhang, H.; Shi, L.; Ye, J. Co-Porphyrin/Carbon Nitride Hybrids for Improved Photocatalytic CO_2 Reduction under Visible Light. *Appl. Catal. B Environ.* **2017**, *200*, 141−149.
(39) Zhou, M.; Wang, S.; Yang, P.; Huang, C.; Wang, X. Boron Carbon Nitride Semiconductors Decorated with CdS Nanoparticles for Photocatalytic Reduction of CO_2. *ACS Catal.* **2018**, *8* (6), 4928−4936.
(40) Li, Y.; Li, B.; Zhang, D.; Cheng, L.; Xiang, Q. Crystalline Carbon Nitride Supported Copper Single Atoms for Photocatalytic CO_2 Reduction with Nearly 100% CO Selectivity. *ACS Nano* **2020**, *14* (8), 10552−10561.
(41) Zhou, M.; Wang, S.; Yang, P.; Luo, Z.; Yuan, R.; Asiri, A. M.; Wakeel, M.; Wang, X. Layered Heterostructures of Ultrathin Polymeric Carbon Nitride and $ZnIn_2S_4$ Nanosheets for Photocatalytic CO_2 Reduction. *Chem. − Eur. J.* **2018**, *24* (69), 18529−18534, DOI: 10.1002/chem.201803250.
(42) Huang, P.; Huang, J.; Pantovich, S. A.; Carl, A. D.; Fenton, T. G.; Caputo, C. A.; Grimm, R. L.; Frenkel, A. I.; Li, G. Selective CO_2 Reduction Catalyzed by Single Cobalt Sites on Carbon Nitride under Visible-Light Irradiation. *J. Am. Chem. Soc.* **2018**, *140* (47), 16042−16047.
(43) Chen, P.; Lei, B.; Dong, X.; Wang, H.; Sheng, J.; Cui, W.; Li, J.; Sun, Y.; Wang, Z.; Dong, F. Rare-Earth Single-Atom La−N Charge-Transfer Bridge on Carbon Nitride for Highly Efficient and Selective Photocatalytic CO_2 Reduction. *ACS Nano* **2020**, *14* (11), 15841−15852.
(44) Li, F.; Yue, X.; Zhang, D.; Fan, J.; Xiang, Q. Targeted Regulation of Exciton Dissociation in Graphitic Carbon Nitride by Vacancy Modification for Efficient Photocatalytic CO_2 Reduction. *Appl. Catal., B* **2021**, *292*, No. 120179.
(45) Pauly, M.; Deegbey, M.; Keller, L.; McGuigan, S.; Dianat, G.; Wong, J. C.; Murphey, C. G. F.; Shang, B.; Wang, H.; Cahoon, J. Catalytic CO2 Reduction Using an Atomically Precise, Cu-Coordinated. *Cambridge Open Engage: Crystalline Carbon Nitride*; ChemRxiv: Cambridge; 2023.

https://doi.org/10.1021/acsaem.3c01670
ACS Appl. Energy Mater. 2023, 6, 10542−10553